Available online at www.sciencedirect.com
ScienceDirect
Journal of Sound and Vibration 313 (2008) 57–76
JOURNAL OF SOUND AND VIBRATION
www.elsevier.com/locate/jsvi

Application of broadband nonlinear targeted energy transfers for seismic mitigation of a shear frame: Experimental results

F. Nucera[a,*], F. Lo Iacono[a], D.M. McFarland[b], L.A. Bergman[b], A.F. Vakakis[c,d,e]

[a]*Department of Mechanics and Materials, Mediterranean University of Reggio Calabria, Via Graziella, Feo di Vito, 89122 Reggio Calabria, Italy*
[b]*Department of Aerospace Engineering, University of Illinois at Urbana-Champaign, Urbana, IL, USA*
[c]*Division of Mechanics, National Technical University of Athens, Greece*
[d]*Department of Mechanical and Industrial Engineering (adjunct), University of Illinois at Urbana-Champaign, IL, USA*
[e]*Department of Aerospace Engineering (adjunct), University of Illinois at Urbana-Champaign, IL, USA*

Received 4 May 2007; received in revised form 29 October 2007; accepted 6 November 2007
Handling Editor: C. Morfey
Available online 4 March 2008

Abstract

In an earlier work we showed computationally that it is possible to successfully employ nonlinear targeted energy transfers (TETs) for seismic mitigation. Moreover, we demonstrated that this passive strategy of seismic vibration control was feasible and robust. In this work, we report experimental validation of these results by performing a series of experimental tests with a three-story shear-frame structure under seismic excitation in the form of two different historic earthquakes. As in the computational part of this work, the experimental seismic mitigation design consists of either a single nonlinear energy sink or a combination of two nonlinear energy sinks (NESs) attached at floors of the test structure. We study the performance and efficiency of the NES(s) through a set of certain evaluation criteria. With a single vibro-impact NES (VI NES) applied to the top floor of the test structure, we find significant reduction of the response levels. To further improve the effectiveness of the seismic mitigation design, we consider a combination of two NESs—an NES with smooth stiffness nonlinearity at the top floor and a VI NES at the bottom floor of the test structure—and show dramatic reduction of the structural seismic response. Robustness of the proposed designs is addressed.

1. Introduction

In the context of seismic risk mitigation, it is crucial to be able to dissipate in the shortest possible time the seismic energy imparted to a structure by an earthquake. This becomes clear when one recognizes that, for a typical seismic excitation, the most severe loads occur in the initial few cycles of the structural response. The concept of nonlinear energy pumping, or targeted energy transfer (TET) [1,2], can be applied in designs for efficient seismic mitigation. By TET we denote the one-way (on the average, i.e. although there is some backscattering of energy from the nonlinear energy sink (NES) to the linear structure, on the average there is

*Corresponding author. Tel.: +39 965 875 221.
E-mail address: francesco.nucera@unirc.it (F. Nucera).

0022-460X/$ - see front matter © 2007 Elsevier Ltd. All rights reserved.
doi:10.1016/j.jsv.2007.11.018

irreversible inflow of energy from the linear structure to the NES), directed transfer of vibration or shock energy from a main structure to a local attachment with damping and essential stiffness nonlinearity, where the energy is confined and locally dissipated without 'spreading' back to the main structure. The underlying dynamical mechanism governing TET is isolated transient resonance captures (TRCs) [3–5] or cascades of TRCs. By isolated TRC (cascade of TRCs) we denote the transient internal resonance of a local nonlinear attachment with one of (a series of) the modes of the main structure. This provides the necessary conditions for the one-way flow of energy from the structure to the attachment, which then acts as a NES.

As in recent related work [2], the experimental problem discussed in this paper is posed as follows: Design a single or a set of local nonlinear attachments (NESs) to a primary structure, with the purpose of rapidly absorbing and locally dissipating a significant part of the seismic energy of the structure at a sufficiently fast time scale, thus significantly reducing the seismic response of the primary structure in the critical initial cycles, and experimentally demonstrate the effectiveness of this design.

The overall goal will be to demonstrate that it is feasible to passively and rapidly divert the applied seismic energy from the main structure (to be protected) to a nonlinear substructure (the NES) defined a priori, where this energy is locally dissipated at a time scale that is fast enough to be of practical use for seismic mitigation. It is the aim of this work to show experimentally that nonlinear energy pumping is a feasible and robust strategy for seismic mitigation, thus confirming the computational results reported in Ref. [2]. It was shown in an earlier work [1] that it is possible to rapidly extract a significant portion of seismic energy from a single-degree-of-freedom (sdof) primary structure through targeted energy transfers (TETs) to an attached vibro-impact NES (VI NES).

As a preliminary step of the experimental study, we perform experimental modal analysis to estimate the modal parameters of the three-story shear frame with no NES attached. Then, we proceed to attach single or multiple NESs to the frame and to assess their capacity to reduce the structural response during the critical initial cycles after the earthquake excitation begins. We perform optimization studies for selecting the NES parameters, and address robustness issues of the proposed designs.

We consider the novel aspects of this work to be twofold. First, in full agreement with the results reported in Ref. [2], we verify experimentally that the VI NES is capable of extracting and dissipating significant portions of the broadband seismic energy from the main structure, and that it does so sufficiently fast. Second, we experimentally confirm the theoretical prediction [2] that the VI NES excites higher structural modes, and, hence, 'spreads' seismic energy from low- to high-frequency ranges. This proves to be advantageous for seismic mitigation, as higher-frequency structural modes typically possess higher modal damping ratios than lower-frequency ones; in addition (and perhaps even more important), higher-frequency structural modes possess smaller amplitudes of vibration compared to lower-frequency ones, which results in significant reduction of the peak response amplitude of the structure.

2. The experimental fixture

The three-story shear frame depicted in Fig. 1a was built at the Linear and Nonlinear Dynamic Vibration Laboratory (LNDVL) at the University of Illinois at Urbana-Champaign. Spring steel was chosen for the columns, and the floor slabs were polypropylene; sufficiently thick that the floor may be regarded as rigid in the horizontal plane. Thus the frame to reasonably be considered as shear-type; in essence, the frame can be considered as possessing three-degrees of freedom (dofs). In Fig. 1b we depict the geometry of the steel plates used to build the columns; their thickness is 0.76 mm. Eight capscrews were used to fix the columns to each polypropylene plate. The width and length of the polypropylene slabs are the same as those of the steel plates, and their thickness is 25.4 mm (1 in). The effective lateral stiffness of each column has been computed, considering clamped–clamped boundary conditions, as

$$k = \frac{12EI}{h^3}, \tag{1}$$

where E is Young's modulus, I the moment of inertia of the cross section, and h the effective length of the column; this leads to an approximate value of $k = 5000\,\mathrm{N/m}$. The connections between floor slabs and the

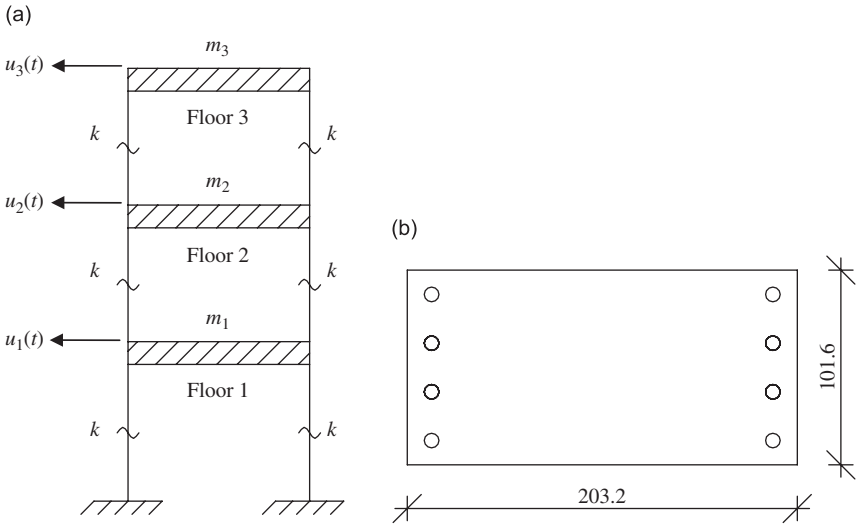

Fig. 1. Schematics of (a) the three-story (three-dof) shear frame and (b) the steel plate employed for the columns.

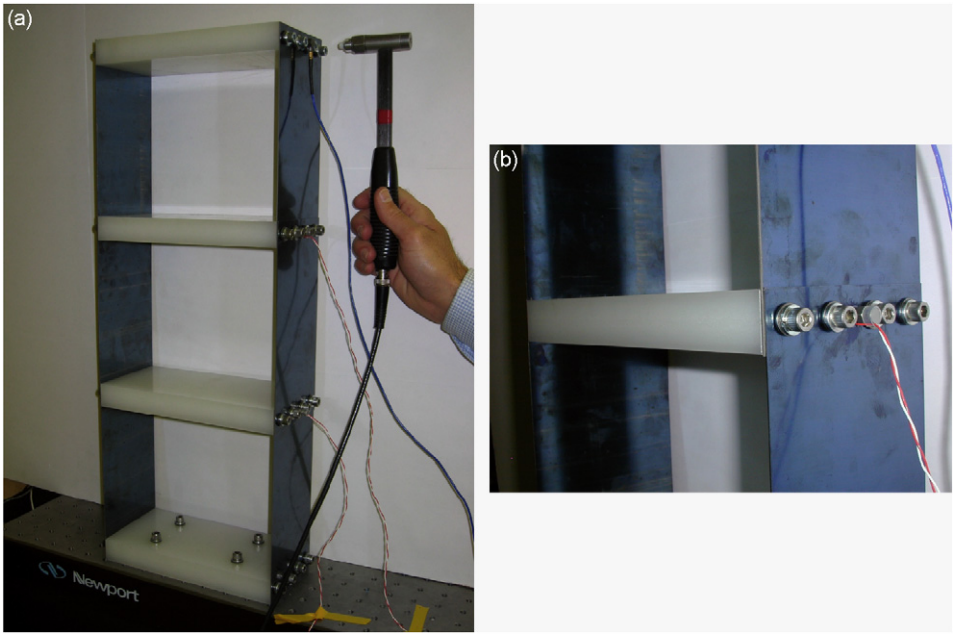

Fig. 2. Instrumentation for modal analysis: (a) frame equipped with accelerometers and impact hammer and (b) accelerometer placement.

columns of the frame were reinforced by applying small aluminum plates. The masses of the three floors of the shear frame were $m_1 = 0.755\,\text{kg}$, $m_2 = 0.755\,\text{kg}$ and $m_3 = 0.634\,\text{kg}$.

Experimental modal analysis was performed to identify the modal parameters of the frame. This was performed by exciting the frame using an impulse hammer, and measuring the corresponding responses at the floors by means of three accelerometers (cf. Fig. 2). Additional data acquisition equipment included a signal conditioner and a SigLab analog-to-digital converter (ADC). A series of five tests was performed for each excitation point, at a sampling frequency of 512 Hz and number of samples recorded equal to 8192. Velocity and displacement time series were computed by numerically integrating the directly measured acceleration time series. In doing this, a suitable high pass filter was applied.

Table 1
Experimental modal parameters of the shear frame

ITD						RFP					
Mode	dof			Freq. (Hz)	Damping ratio (%)	Mode	dof			Freq. (Hz)	Damping ratio (%)
	1	2	3				1	2	3		
1	0.32	0.87	1.00	4.82	0.291	1	0.35	0.91	1.00	4.82	0.257
2	1.00	0.32	−0.94	12.69	0.311	2	1.00	0.32	−0.90	12.70	0.314
3	−0.65	1.00	−0.58	18.12	0.230	3	−0.65	1.00	−0.56	18.14	0.242

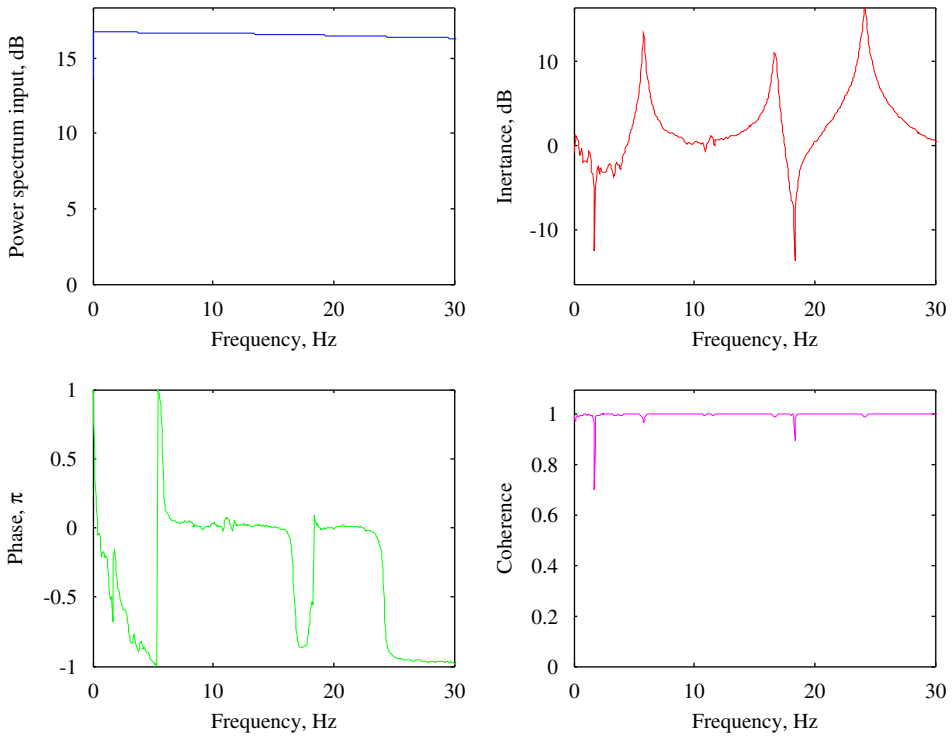

Fig. 3. Frame with no NES attached, typical FRF experimental measurement: input power spectrum, cross FRF magnitude and phase, and coherence.

Experimental modal analysis was performed by employing two different techniques [6]. The Ibrahim time domain (ITD) algorithm is based in the time domain and directly analyzes free-response time histories from the structure under test, whereas the rational fraction polynomial (RFP) curve fit algorithm is based in the frequency domain and estimates the modal parameters by curve fitting experimental frequency response functions (FRFs). The modal analysis results obtained by these methods are similar, and are summarized in Table 1. The modal analysis was performed assuming linearity; the linear behavior of the test structure was checked by computing the coherence function

$$\gamma^2(f) = \frac{|G_{xy}(f)|^2}{G_{xx}(f)G_{yy}(f)}, \tag{2}$$

where $G_{xy}(f)$ represents the cross power spectrum between the excitation and the response signal, $G_{xx}(f)$ the power spectrum of the excitation signal, $G_{yy}(f)$ the power spectrum of the response signal, and f the frequency.

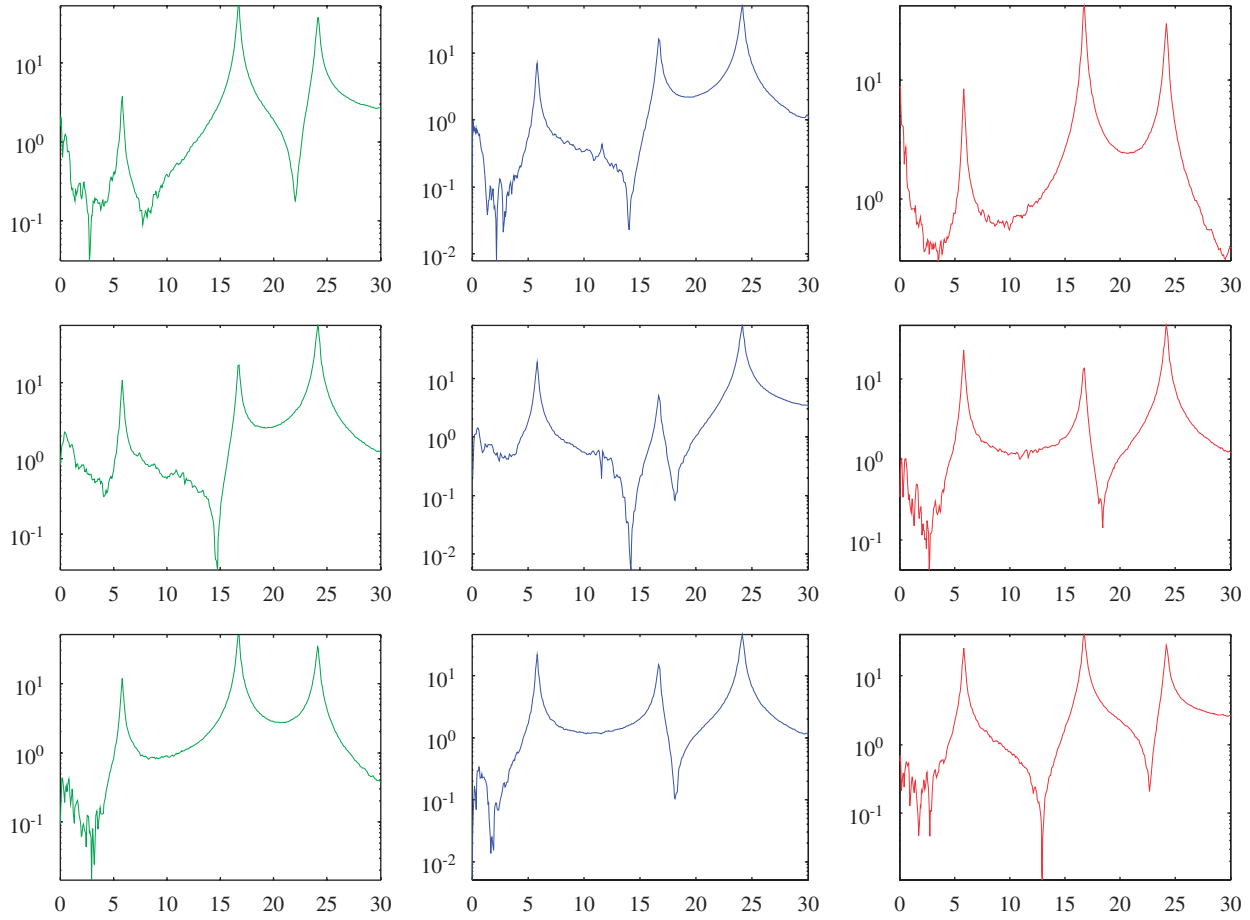

Fig. 4. Frame with no NES attached: experimental (3 × 3) FRF matrix.

Fig. 3 depicts a typical cross FRF corresponding to excitation applied at the third floor and response measured at the second floor; the measurement was restricted to the frequency range of interest. In Fig. 4 we present the full (3 × 3) experimentally measured FRF matrix for the test structure. A force window has been used for the excitation signal whereas for the response signal an exponential window was applied. As seen from the depicted results, the energy of the impulse is fairly even over the frequency range of interest. Moreover, the coherence function is nearly equal to unity over the entire frequency range of interest, with the exception of antiresonances, where the signal-to-noise ratio is low. We note that the identified modal damping ratios are used in our search for optimal parameters (e.g., clearance, mass ratio) for the VI NES that will be attached to the frame.

3. Design I: single VI NES attached to the top floor of the frame

We now study the dynamical response of the three-dof shear frame excited by two historical earthquakes. In particular, we will focus our attention on (i) the Kobe earthquake, N–S component recorded at the Kobe Japanese Meteorological Agency (JMA) station during the Hyogo-ken Nanbu earthquake of January 17, 1995; and (ii) the Northridge earthquake, N–S component recorded at the Sylmar County Hospital parking lot in Sylmar, California, during the Northridge, California earthquake of January 17, 1994. Both of these earthquakes are characterized by relatively short effective ground motion duration and large values of peak ground acceleration (PGA), peak ground velocity (PGV), effective peak acceleration (EPA), and effective

peak velocity (EPV). These are intensity measures (IMs) used to describe the severity of an earthquake, either directly in terms of its time series characteristics, or in terms of its effect on a structure.

The PGA IM is defined as

$$\mathrm{PGA} = \max|\ddot{u}_g(t)|, \tag{3}$$

where $\ddot{u}_g(t)$ denotes ground motion and overdot, differentiation with respect to time. Likewise, the second IM is defined as

$$\mathrm{PGV} = \max|\dot{u}_g(t)|. \tag{4}$$

Some IMs are based on the earthquake (shock) response of a sdof system considered as a low-pass filter. The traditional IM of spectral quantity (displacement, velocity or acceleration) is defined by considering the governing equation of motion of a linear sdof oscillator subject to ground acceleration $\ddot{u}_g(t)$, $\ddot{u} + 2\xi\omega_n\dot{u} + \omega_n^2 u = -\ddot{u}_g(t)$ where ξ and $\omega_n = 2\pi/T_n$ are the critical damping ratio and natural frequency, respectively. It follows that the response is a function of these parameters, $u \equiv u(t, T_n, \xi)$, with the damping ratio conventionally used for the earthquake IMs of the order of 5%. The response spectrum provides a convenient way to summarize the peak response of all possible linear sdof systems to a particular component of ground motion. A plot of the peak value of a response quantity as a function of the natural vibration period T_n of the system, or a related parameter such as circular frequency ω_n or cyclic frequency f_n, is called the response spectrum for that quantity. Considering different response quantities, such as displacement, velocity and acceleration, one can define different spectra as follows: the spectral displacement (D) is given by

$$\begin{aligned} D = u_0(T_n, \xi) &\equiv \max_t |u(t, T_n, \xi)|, \\ \dot{u}_0(T_n, \xi) &\equiv \max_t |\dot{u}(t, T_n, \xi)|, \\ \ddot{u}_0(T_n, \xi) &\equiv \max_t |\ddot{u}(t, T_n, \xi)|. \end{aligned}$$

For a sdof system with natural frequency ω_n the spectral velocity (V) is defined as $V = \omega_n D$ which, when plotted against T_n, defines the pseudo-velocity response spectrum. The prefix 'pseudo' means that V is not identical to the peak velocity of the system, $\dot{u}_0(T_n, \xi)$, although it has the correct units. Likewise, the spectral acceleration (A) $A = \omega_n V$ plotted versus T_n, defines the pseudo-acceleration response spectrum. Again, the term pseudo-acceleration is used to differentiate A from the peak acceleration of the system, $\ddot{u}_0(T_n, \xi)$, although it has the correct units.

Based on the concept of response spectrum, we consider the EPA described by the formula

$$\mathrm{EPA} = \frac{A(T_i, \xi)|_{0.1}^{T_n=0.5}}{2.5}. \tag{5}$$

This represents the mean value of the pseudo-acceleration response spectrum (for damping ratio 5%) for the periods between 0.1 and 0.5 s divided by a standard amplification coefficient of 2.5. Similarly, the EPV is the mean value of the pseudo-velocity response spectrum (for damping ratio 5%) for the periods between 0.7 and 2 s divided by a standard amplification coefficient of 2.5:

$$\mathrm{EPV} = \frac{V(T_i, \xi)|_{0.7}^{T_n=2.0}}{2.5}. \tag{6}$$

In addition, the strong motion duration T_D is defined as the time interval of the earthquake record in which the energy transmitted by the earthquake to the structure diminishes from 95% to 5% of its total value I_A; the strong motion duration is computed according to the expression

$$T_D = t(0.95I_A) - t(0.05I_A). \tag{7}$$

The last IM used here was introduced by Fajfar et al. [7] and is known as the medium period (I); this is defined according to the expression

$$I = \mathrm{PGV}(T_D^{0.25}). \tag{8}$$

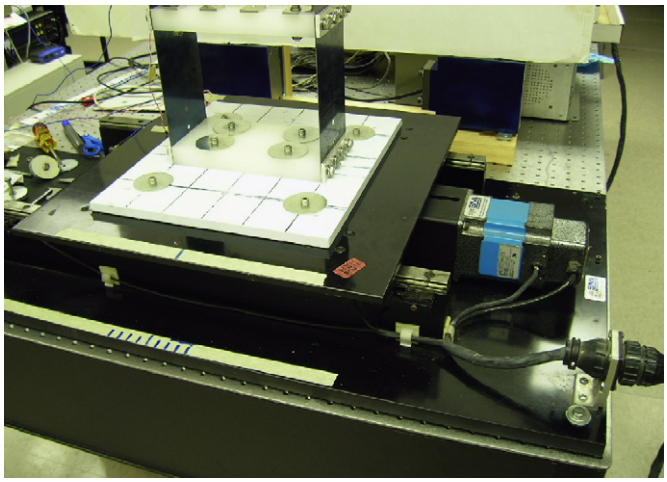

Fig. 5. Electro-mechanical shake table for seismic excitation of the frame.

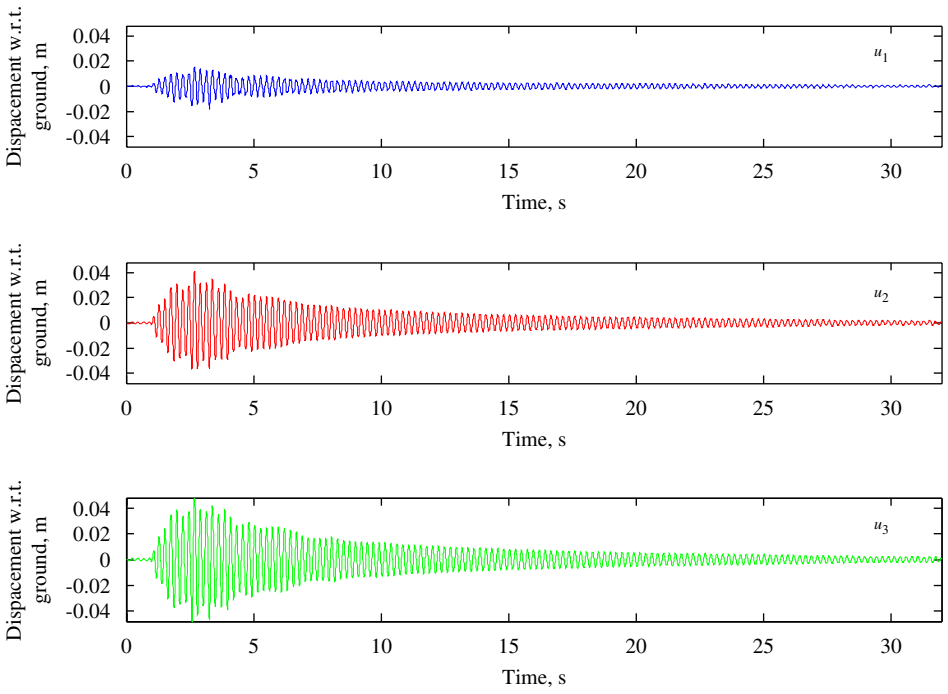

Fig. 6. Displacements with respect to ground of the shear frame excited by the Kobe earthquake—uncontrolled responses.

This is an intensity parameter which can be applicable to ground motions possessing different durations and frequency contents, as well as varying soil conditions. Moreover, Eq. (8) is an instrumental measure of the earthquake ground motion's capacity to damage structures with fundamental period lying in the medium-period range. This region is considered to be very important for two reasons: first, the fundamental periods of the majority of modern buildings usually lie in this region; and second, the dynamic amplifications of the corresponding structural response are expected to attain their highest values in this region.

Comparing the Kobe and Northridge earthquakes, Kobe has the higher energy content (I_A is 67%), both have approximately the same PGA, and Kobe has 10% smaller EPA but 6% greater EPV. Both earthquakes will pose demanding base acceleration input to a structure, resulting in severe seismic forcing; for more detailed descriptions of the characteristics of these historic earthquakes the reader is referred to the companion

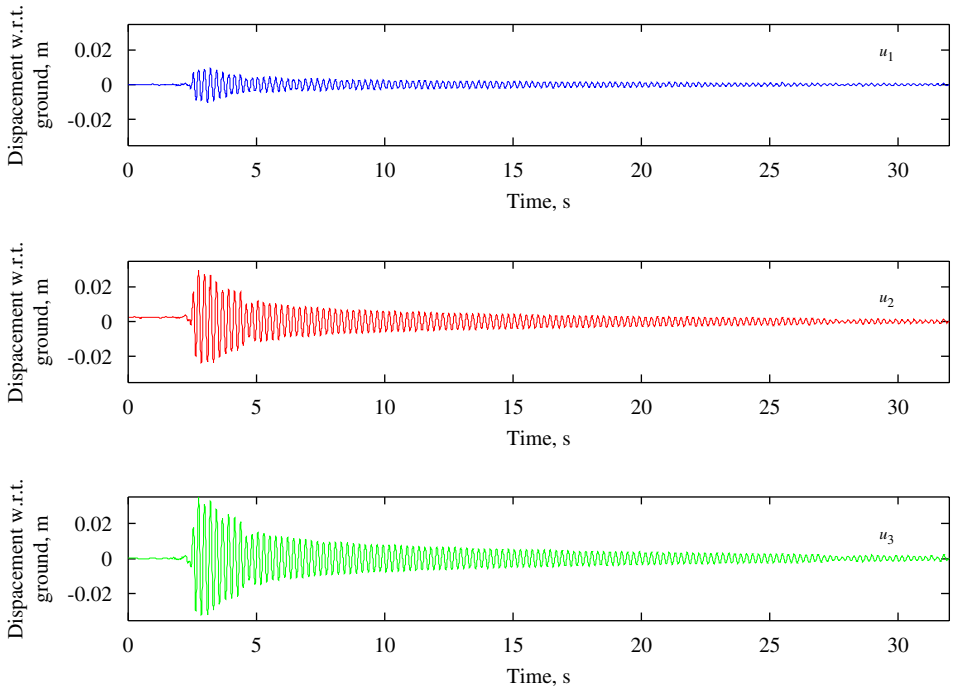

Fig. 7. Displacements with respect to ground of the shear frame excited by the Northridge earthquake—uncontrolled responses.

paper [2]. In addition, in order to 'tune' the earthquake frequency content to the range of the natural frequencies of the linear test structure (and, thus, to make the applied seismic excitation as severe as possible for the test structure), the historic earthquake records were time scaled to 25 s from the original duration of 50 s (as in Ref. [2]).

The experimental seismic excitation was performed by mounting the frame on an electro-mechanical shake table, as depicted in Fig. 5. In Figs. 6 and 7, respectively, we present the responses (floor displacements with respect to ground) of the frame subjected to the Kobe and Northridge earthquakes when no NES was attached. From now on, we will refer to these as uncontrolled responses.

In the first seismic mitigation design (referred to as 'Design I'), we apply a single VI NES at the top floor of the frame. A schematic of Design I is shown depicted in Fig. 8a, and the actual experimental fixture is presented in Fig. 8b. The VI NES consists of a small mass clamped to a shaft allowed to move horizontally in linear ball bearings, and two restrictors which inelastically impact the bearing housings.

As a first step, we perform a computational optimization study in order to tune the parameters of the sink (i.e., clearance e, stiffness k_{NES}, mass m_{NES} and coefficient of restitution for inelastic impacts cr—cf. Fig. 8a) for optimal performance (i.e., optimal TET of seismic energy from the frame). In this particular case we select two different VI NES configurations with mass ratios of 2.5% and 3.5% of the total mass of the frame, respectively. The criteria employed as quantitative measures of the effectiveness of the seismic mitigation design (and used for the optimization exercise) were introduced in Spencer et al. [8] and are listed in Appendix A. Each criterion is represented as a dimensionless ratio related to a variable representing a certain characteristic of the structural response (e.g., displacement or interstory drift); these variables are computed when the structure is controlled and uncontrolled. Since the controlled variables appear in the numerators whereas the uncontrolled ones in the denominators, effective seismic mitigation dictates that the evaluation criteria be less than unity (in fact, smaller values for these criteria indicate more effective seismic mitigation). Although the goal of the optimization should be to determine the NES parameters for which the smallest possible value for each criterion is achieved, in practical terms we can only optimize the NES parameters that minimize an objective function (OF), defined as $\mathrm{OF} = J_1 + J_2 + J_5 + J_6$. The reader is referred to Ref. [2] for a discussion of the selection of the OF for the optimization procedure, as well as for the details of the genetic

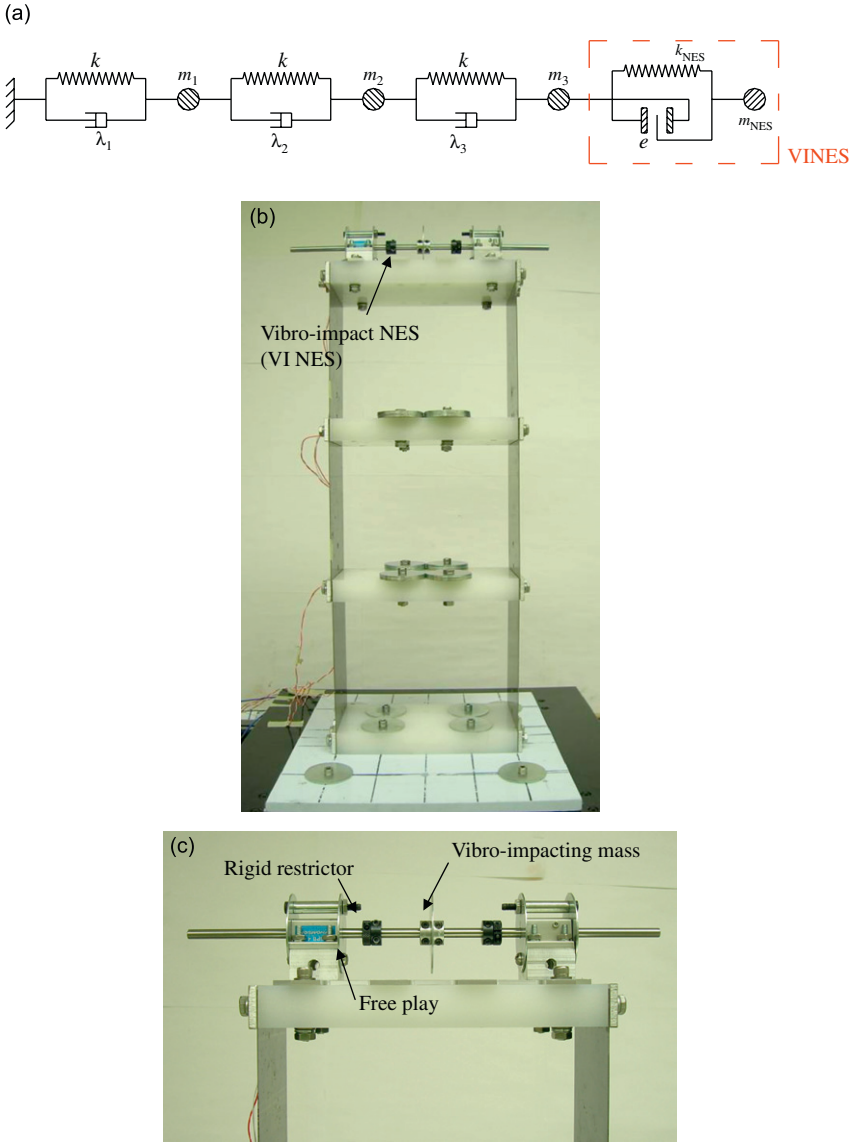

Fig. 8. Design I—frame with VI NES attached to the top floor: (a) schematic, (b) picture, and (c) detail of VI NES.

optimization algorithm. The computational optimization of Design I was carried out for the Kobe seismic excitation (as this corresponded to a more severe excitation to the test fixture compared to the Northridge earthquake) and NES mass ratio equal to 2.5%. The optimized results are $e = 0.024\,\text{m}$, $k_{\text{NES}} = 0.004k$, and $\text{cr} = 0.43$. For an increased NES mass ratio of 3.5%, the optimized parameters are $e = 0.016\,\text{m}$, $k_{\text{NES}} = 0.005k$ and $\text{cr} = 0.42$.

The VI NES implemented in the experimental fixture possesses the parameters determined by this computational optimization study. In Fig. 9 we plot the experimental displacements of each floor with respect to ground for an NES mass ratio of 2.5%. In Fig. 10 we depict the corresponding experimental responses for a fixture with an NES mass ratio of 3.5%. We summarize the results of the experimental tests by stating that for 2.5% NES mass ratio we achieve a remarkable reduction of 31% in terms of maximum displacement with respect to ground, and 30% in terms of maximum interstory drift; these are the structural responses mainly related to structural damage due to seismic excitation. By increasing the NES mass ratio from 2.5% to 3.5% the proposed passive control strategy is further enhanced; in that case we achieve a reduction of 46% in

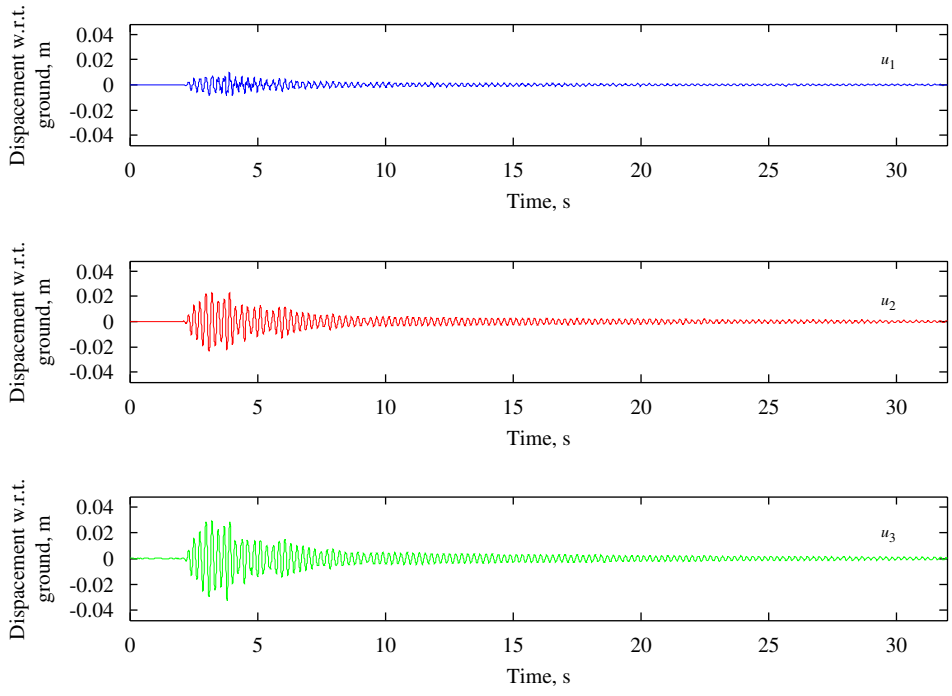

Fig. 9. Experimental responses for optimized Design I, Kobe seismic excitation, NES mass 2.5%.

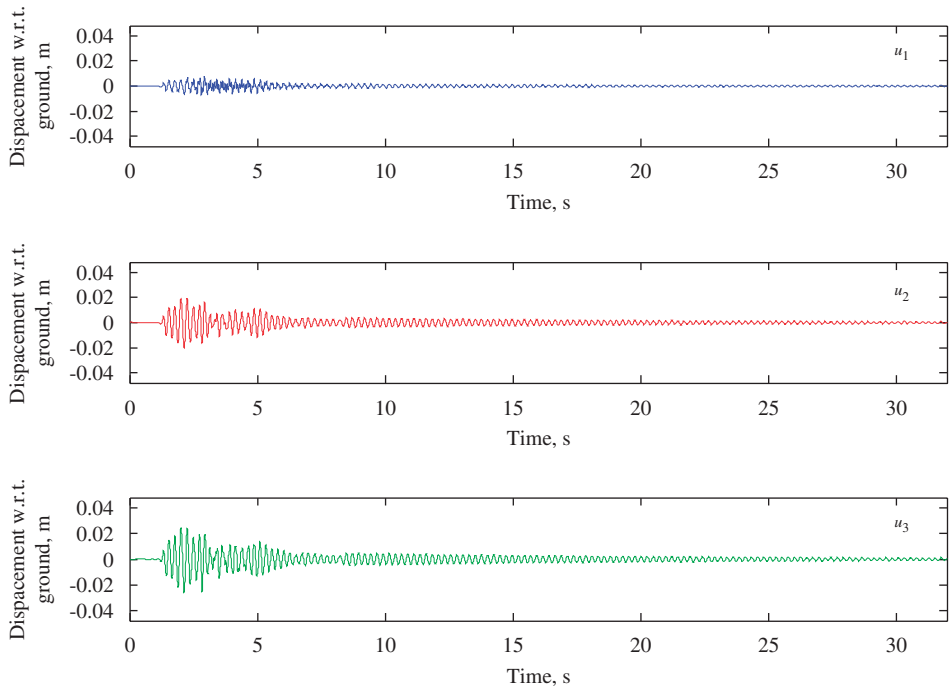

Fig. 10. Experimental responses for optimized Design I, Kobe seismic excitation, NES mass 3.5%.

maximum displacement with respect to ground (compared to the uncontrolled one), and a reduction of 37% in maximum interstory drift. Moreover, we obtain a uniform improvement in virtually all the evaluation criteria, with a maximum of 60% in normed maximum displacement for NES mass ratio 3.5%. The experimental values of all eight evaluation criteria for the optimized Design I are summarized in Table 2.

Table 2
Experimental evaluation criteria (EC), optimized Design I for Kobe seismic excitation

EC	Kobe seismic excitation		Northridge seismic excitation	
	NES mass 2.5%	NES mass 3.5%	NES mass 2.5%	NES mass 3.5%
J_1	0.69	0.54	0.84	0.80
J_2	0.70	0.63	0.87	0.84
J_3	0.89	0.81	0.92	0.88
J_4	0.66	0.57	0.82	0.83
J_5	0.49	0.40	0.54	0.53
J_6	0.50	0.41	0.57	0.56
J_7	0.55	0.54	0.67	0.73
J_8	0.50	0.42	0.57	0.56

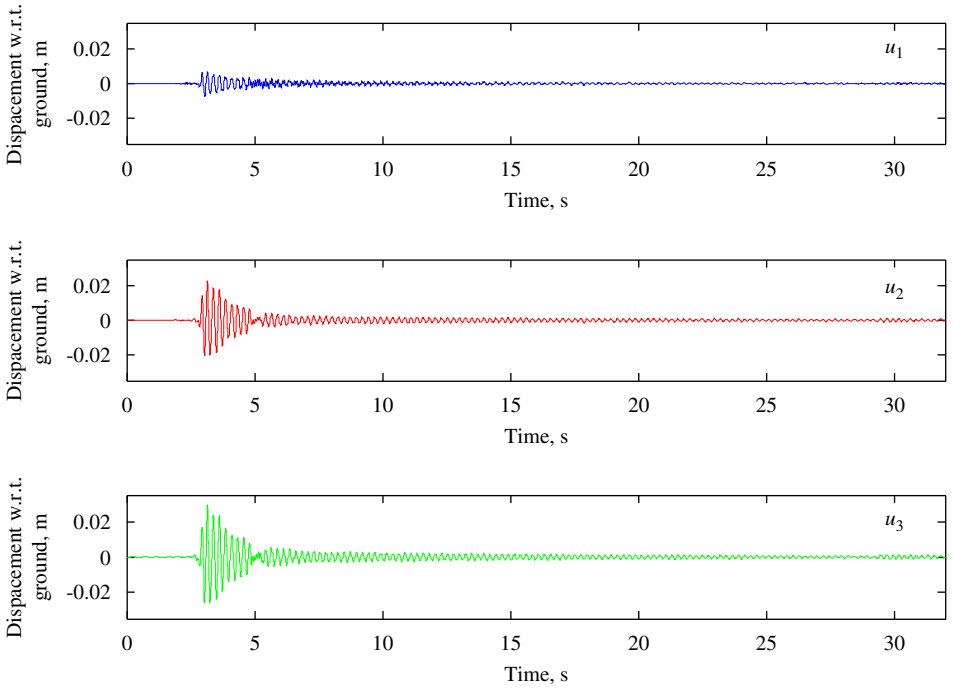

Fig. 11. Experimental responses for optimized Design I, Northridge seismic excitation, NES mass 2.5%.

The optimization of Design I was carried out for the Kobe seismic excitation. To check the performance (i.e., robustness) of this design to an alternative seismic excitation, the frame was subjected to the Northridge seismic excitation (scaled to 25 s duration). The corresponding experimental responses are depicted in Figs. 11 and 12 for NES mass ratios of 2.5% and 3.5%, respectively; the comparison of the experimental values of the evaluation criteria for the Kobe and Northridge cases is provided in Table 2. We note that, although there is still significant reduction in all evaluation criteria under the Northridge seismic excitation, the experimental performance of Design I is less remarkable compared to that achieved for the Kobe record. Nevertheless, reductions of 20% and 16% in maximum displacements with respect to ground (J_1) and maximum interstory drift (J_2), respectively, are still achieved in this case. This outcome should be expected since the optimization of Design I was carried out for a different seismic excitation.

We now study the wavelet spectra of the experimental relative displacements between floors, in order to experimentally verify the spreading of seismic energy from low- to high-frequency modes due to vibro-impacts

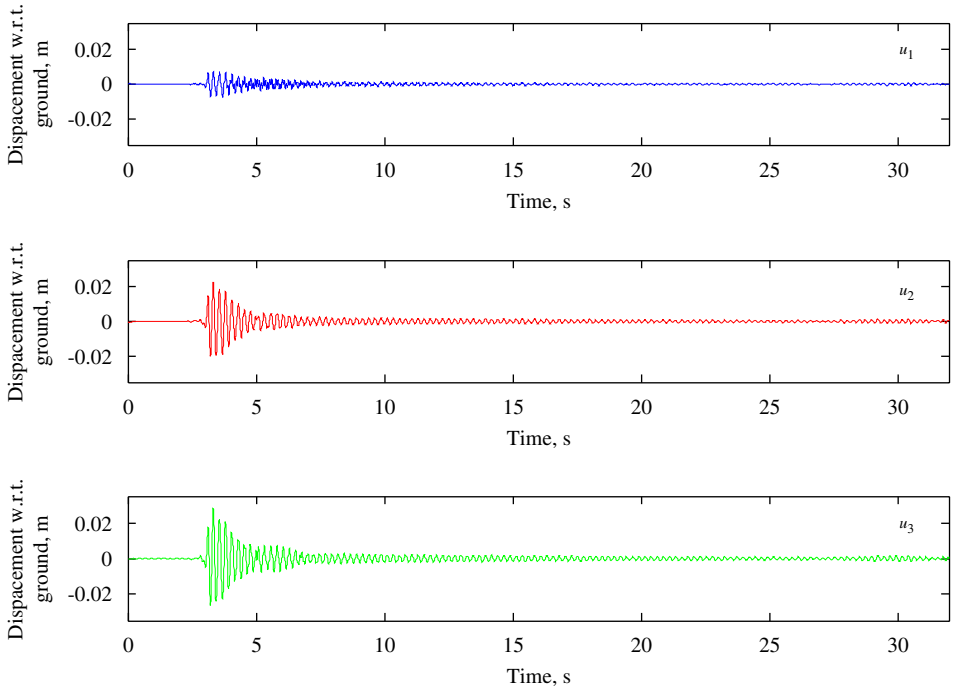

Fig. 12. Experimental responses for optimized Design I, Northridge seismic excitation, NES mass 3.5%.

[2]. The wavelet transform provides the transient evolution of the main frequency components of the experimentally measured time series, and in this work it was performed by a Matlab-based code developed at Université de Liège [9]. The code employs the Morlet mother wavelet, $\psi_M(t) = e^{-t^2/2} e^{j\omega_0 t}$, a Gaussian-windowed complex sinusoid of frequency ω_0 rad/s. The frequency ω_0 is the user parameter which enables one to tune the frequency and time resolution of the results. Herein, the results of applying the numerical wavelet transform are presented in terms of wavelet spectra. These shaded plots depict the amplitude of the wavelet transform as a function of frequency (vertical axis) and time (horizontal axis). Heavily shaded areas correspond to regions where the amplitude of the wavelet transform is high whereas lightly shaded regions correspond to low amplitudes.

In Figs. 13 and 14 we depict the wavelet spectra of the experimental relative displacements between (a) the first floor and ground, $RD_1 = u_1$ (u_1 is the displacement of the first floor with respect to ground); (b) the second and first floors, $RD_2 = u_2 - u_1$; and (c) the third and second floors, $RD_3 = u_3 - u_2$. In these figures we compare the wavelet spectra of the uncontrolled (no VI NES applied) and controlled responses, subject to either Kobe or Northridge seismic excitations. It is clear from these results that the dominant harmonics of the relative displacements occur mainly at the first linearized natural frequency of the frame. This is typical in unprotected structures which, under seismic excitation, usually respond in their lowest mode and so behave approximately as sdof oscillators. This leads, in turn, to relatively large responses.

A qualitatively different result is deduced from the experimental wavelet spectra of Figs. 15 and 16, which analyze the corresponding relative displacements (RD_1, RD_2 and RD_3) of the frame with the VI NES attached at its top floor (Design I). The VI NES used in these experimental results had a mass ratio of 3.5%, and its parameters were provided by the optimization for Kobe seismic excitation. The high-frequency scattering of seismic energy to the second (and some cases even the third) structural mode due to the vibro-impacts at the NES is experimentally verified. For the case of Kobe seismic excitation we note the participation of the second mode and somewhat of the third in the seismic response; whereas, for Northridge seismic excitation there appears mainly a contribution of the second mode in the relative responses. These experimental results confirm the theoretical findings reported in Ref. [2].

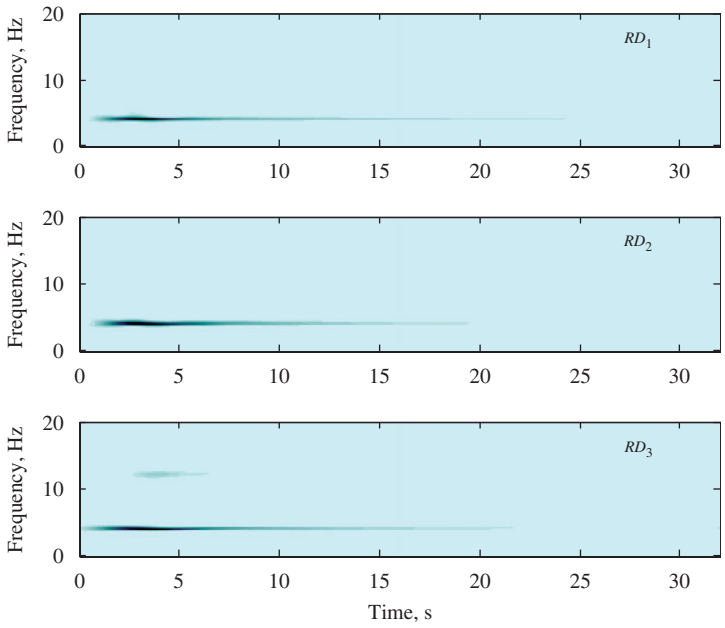

Fig. 13. Experimental wavelet spectra of relative displacements, uncontrolled structure under Kobe excitation.

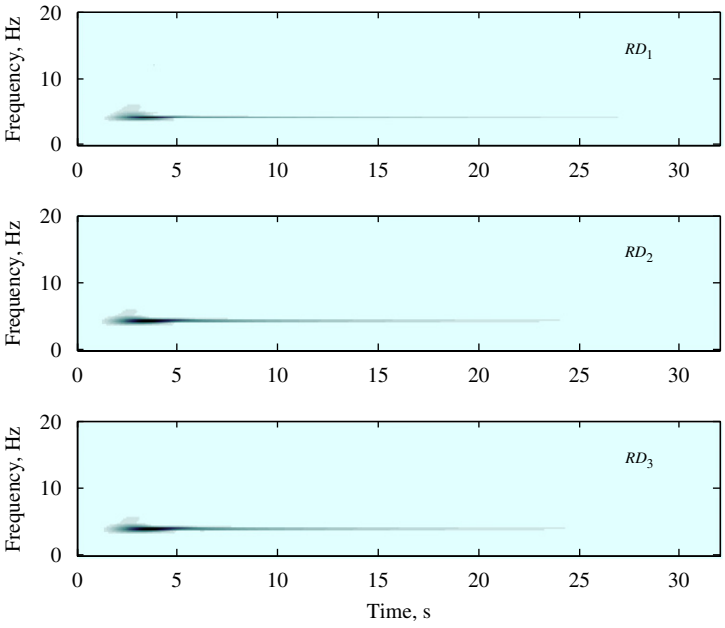

Fig. 14. Experimental wavelet spectra of relative displacements, uncontrolled structure under Northridge excitation.

4. Design II: VI NES connected at the bottom floor and smooth NES connected at the top floor of the shear frame

Usually, seismically excited structures experience large displacements and, hence, suffer structural damage during strong ground motion. Therefore, from the point of view of seismic protection it becomes crucial to reduce the response of the initial cycles of vibration. We showed that a single VI NES attached to the top floor

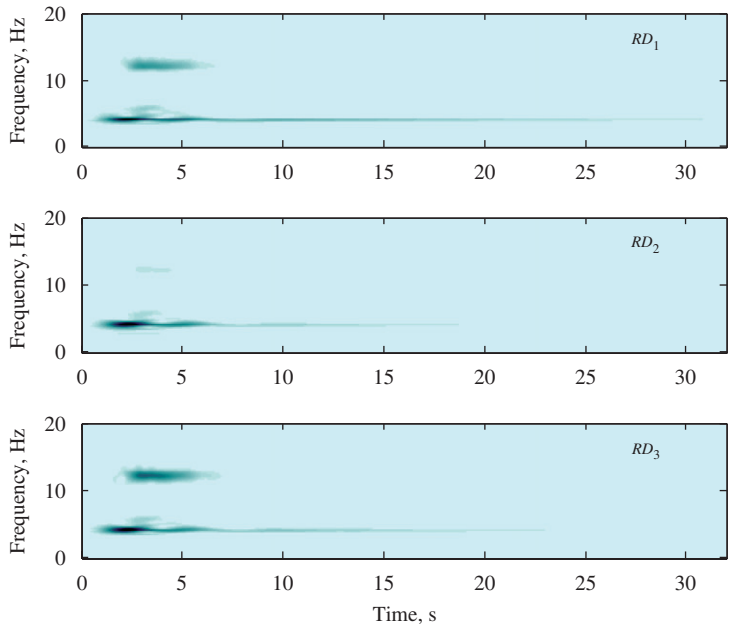

Fig. 15. Experimental wavelet spectra of relative displacements, optimized Design I (3.5% VI NES ratio), Kobe excitation.

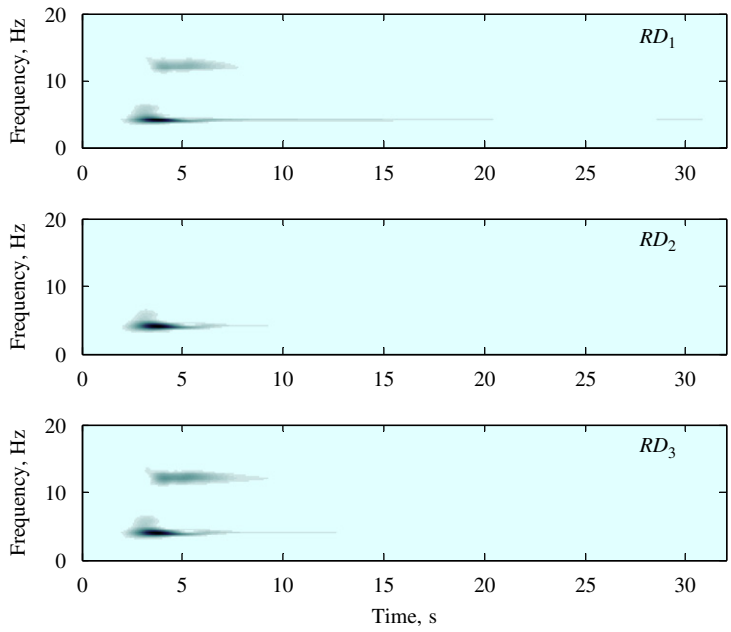

Fig. 16. Experimental wavelet spectra of relative displacements, optimized Design I (3.5% VI NES ratio), Northridge excitation.

is capable of acting at sufficiently fast time scale (just at the beginning of the strong ground motion), resulting in a significant reduction of the structural response peaks. After this initial stage of the structural response, the amplitudes of vibration reach lower levels; consequently the relative displacements between floors and between the VI NES and the floor to which it is attached become smaller, as well, until no vibro-impacts occur. Therefore, in Design I, one should take into account the possibility of absence of vibro-impacts after the initial stage of the motion; i.e., of the complete absence of control action by the VI NES. For this reason, we consider

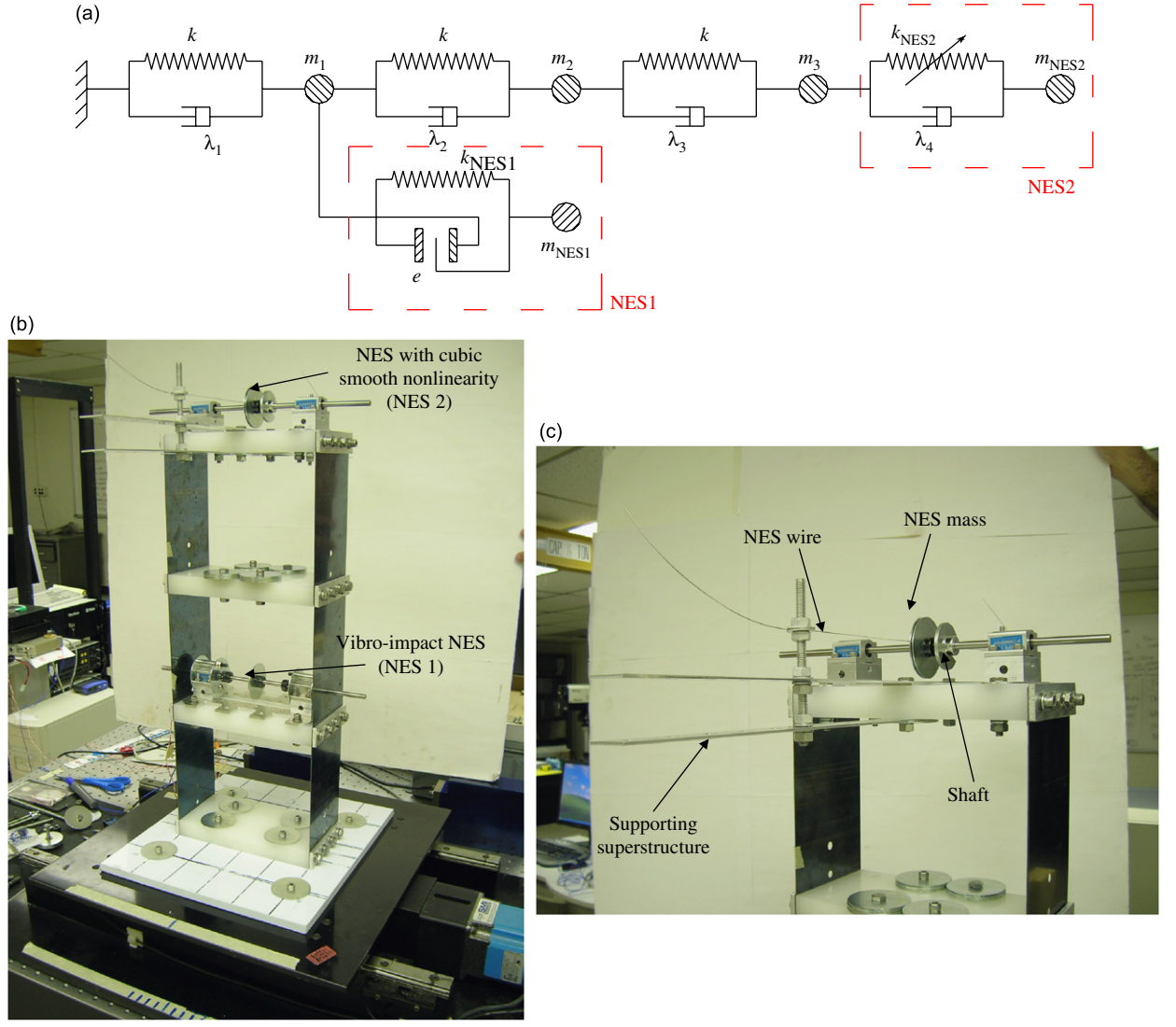

Fig. 17. Design II—frame with VI NES (NES 1) attached at the bottom floor, and NES with cubic essential nonlinearity (NES 2) at the top floor: (a) schematic, (b) picture, and (c) detail of NES 2.

an alternative design, based on the use of a combination of NESs capable of providing seismic control during both initial high-amplitude, and later lower-amplitude, regimes of the structural response. Design II consists of a VI NES attached at the bottom floor (labeled 'NES 1'), and an NES with smooth (cubic) essential stiffness nonlinearity (labeled 'NES 2') at the top floor of the shear frame. The VI NES is designed to provide vibration control mainly in the initial high-amplitude regime of the structural response, and the NES with smooth stiffness nonlinearity, to reduce the amplitude of the motion in the later, lower-amplitude regime. A schematic and a picture of Design II are shown in Fig. 17a and b. In Fig. 17c we show a detail of NES 2. It consists of a mass fixed to a shaft supported by linear bearings and restricted in its motion by a perpendicular wire with no pretension. As discussed in Ref. [10], the force exerted by the wire on the shaft during its motion is essentially nonlinear (it possesses approximately a cubic force–deformation relationship with no linear term).

The parameters of NES 2 that need to be optimized (in addition to those relevant to the VI NES—coupling stiffness, k_{NES1}, clearance e, and coefficient of restitution cr) are the damping constant λ_4, and the coefficient of the nonlinear cubic stiffness nonlinearity, k_{NES2}. For the experimental Design II we assume that the mass of each of the two NESs is fixed at 2.5% of the mass of the frame. By employing the optimization

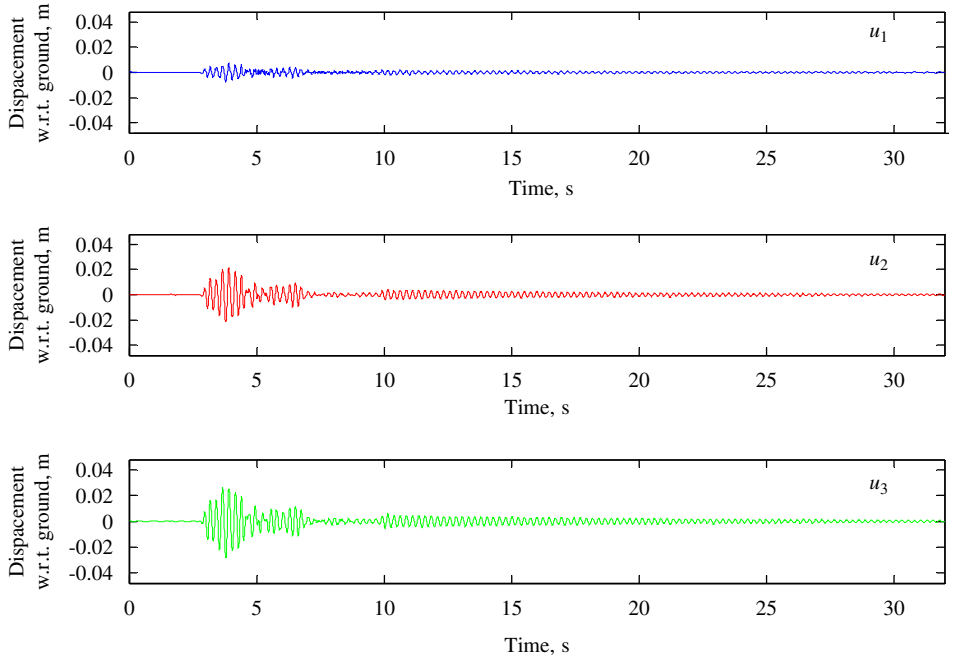

Fig. 18. Experimental responses for optimized Design II, Kobe seismic excitation.

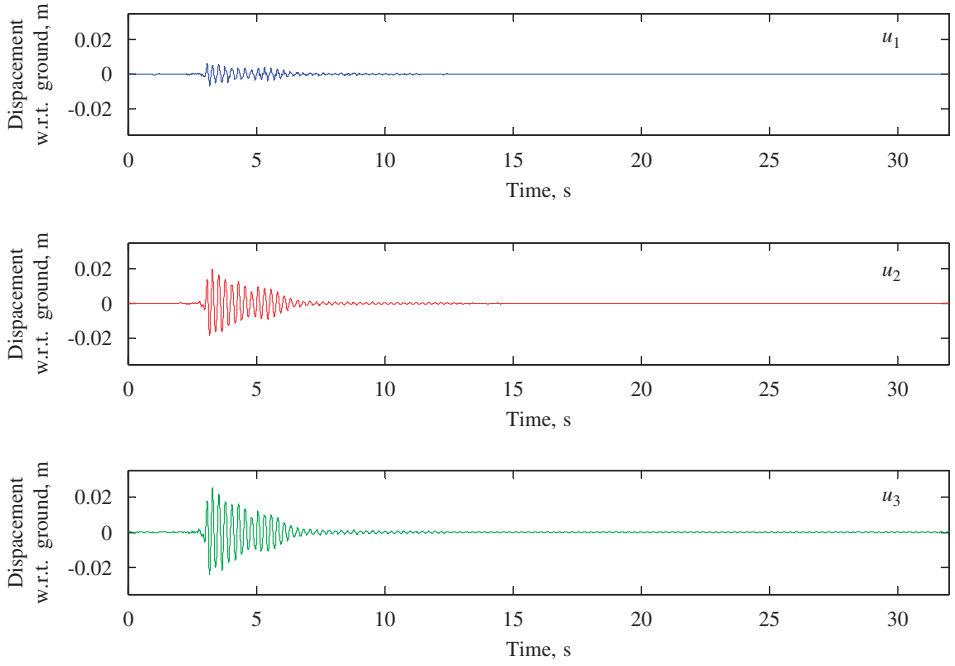

Fig. 19. Experimental responses for optimized Design II, Northridge seismic excitation.

approach described in Section 3, we obtain the following values for the parameters, under Kobe seismic excitation: (i) for the VI NES (NES 1), $e = 0.012\,\mathrm{m}$, $\mathrm{cr} = 0.43$ and $k_{\mathrm{NES1}} = 0.003k$; (ii) for the smooth sink (NES 2), $k_{\mathrm{NES2}}/k = 16\,\mathrm{m}^{-2}$ and $\lambda_4/\lambda_3 = 2.8$.

In Figs. 18 and 19 we show the experimental displacements with respect to ground of the frame implementing Design II with the optimized parameters, and subject to Kobe and Northridge seismic

excitations, respectively. The seismic mitigation performance of this control strategy is evaluated through the eight criteria which are summarized in Table 3. Focusing first on the case of Kobe excitation, we note that there is a dramatic attenuation of the structural responses during both the early stage of the motion (i.e., under condition of strong ground motion) and the later stage (after 15 s, when almost all the seismic energy has been released by the ground motion). Indeed, we achieve reductions of 41% and 38% in maximum displacement with respect to ground, and maximum interstory drift, respectively. If we compare the later stage (lower-amplitude) performance for Designs I and II, we note that the maximum displacement (J_1 criterion) is slightly higher with Design II. On the other hand, NES 2 in Design II provides an important contribution in reducing the normed criteria, (i.e., J_5–J_8); in fact all these criteria are remarkably smaller compared to those achieved by Design I. The wavelet spectra of the relative displacements, depicted in Figs. 20 and 21, are proof of the beneficial effects to seismic mitigation provided by the action of the VI NES, as explained in the previous section. In fact, it appears that in Design II there is more vigorous seismic energy scattering to higher-frequency modes, compared to Design I (cf. Figs. 13–16).

Table 3
Experimental evaluation criteria (EC), optimized Design II for Kobe seismic excitation

EC	Kobe seismic excitation VI NES mass 2.5% SM NES mass 2.5%	Northridge seismic excitation VI NES mass 2.5% SM NES mass 2.5%
J_1	0.56	0.73
J_2	0.62	0.82
J_3	0.51	0.85
J_4	0.55	0.81
J_5	0.38	0.53
J_6	0.39	0.57
J_7	0.37	0.64
J_8	0.34	0.56

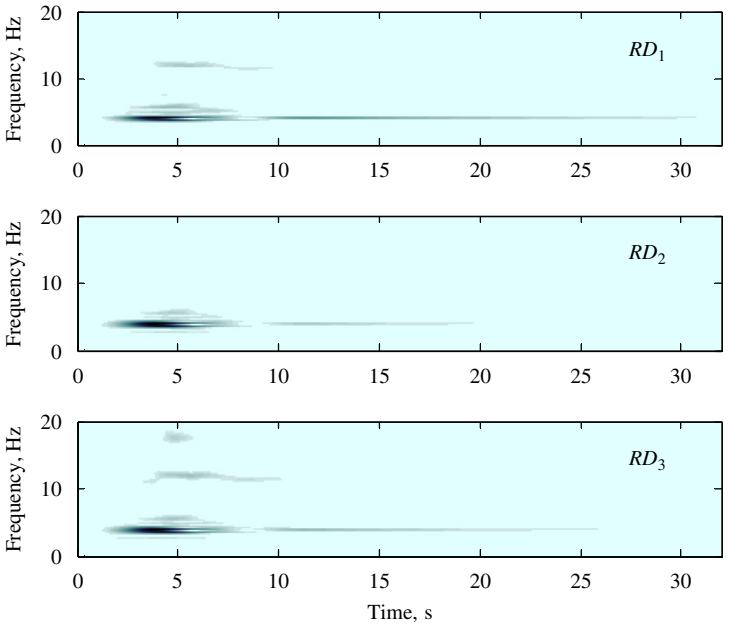

Fig. 20. Experimental wavelet spectra of relative displacements, optimized Design II, Kobe excitation.

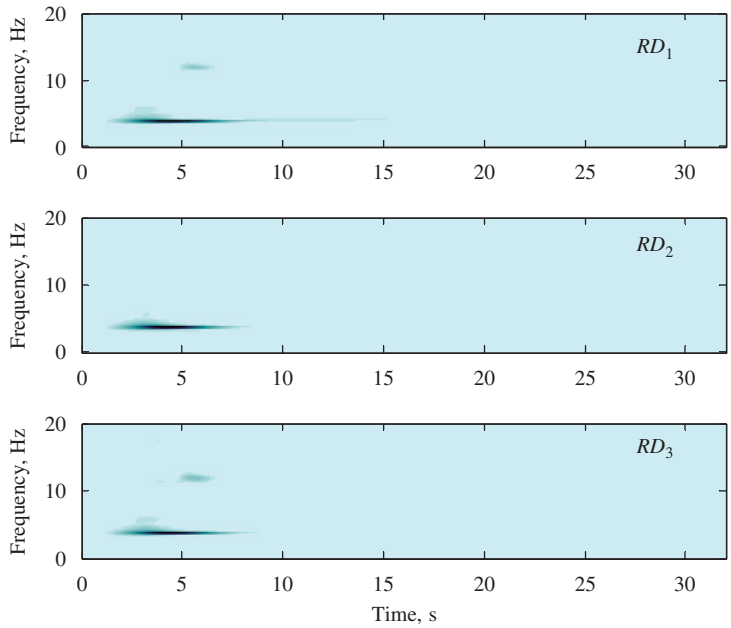

Fig. 21. Experimental wavelet spectra of relative displacements, optimized Design II, Northridge excitation.

The NES parameters optimized for the Kobe earthquake were also employed to test the robustness of Design II subject to Northridge earthquake excitation. We note a general performance improvement in terms of both normed and un-normed criteria; however, criteria J_6 and J_8 are nearly identical to Design I.

5. Concluding remarks

In this work, we showed that lightweight, essentially nonlinear, passive attachments can be designed to significantly reduce the peak amplitudes of the seismic response in the critical initial stage of structural motion, during the regime of strong ground motion. Two different NES designs were considered in this work, based on the use of either a single VI NES on the top floor (Design I), or a combination of a VI NES on the lowest floor and an NES with smooth essential stiffness nonlinearity on the top floor (Design II).

The use of VI NESs is dictated by previous theoretical predictions [11,12] (and experimental demonstrations of these predictions herein) that a VI NES is capable of acting sufficiently quickly to reduce the amplitude peaks of the structural response which occur during strong ground motion, when the seismic energy input is at its highest and the potential for structural damage is at its greatest. In addition, vibro-impacts induced by the NES scatter seismic energy from lower- to higher-frequency structural modes; as a result, the responses of the structure are significantly reduced, because higher structural modes generally exhibit lower amplitudes of vibration and dissipate energy more efficiently.

The rationale of using a combination of NESs with smooth and nonsmooth nonlinearities (Design II) follows from the results of previous works [6,8,9–11] which showed that NESs with smooth, essential stiffness nonlinearities are capable of passively absorbing and locally dissipating seismic energy, especially when their mass is relatively light; moreover, at higher floors the level of structural vibration is higher, which facilitates the activation of the essential stiffness nonlinearity of this type of NES. Furthermore, an NES with essential (nonlinearizable) stiffness nonlinearity is capable of resonating with any of the structural modes, as it does not possess any preferential resonance frequency; it follows that such a local attachment can have global effects on the structural dynamics.

By performing optimization studies by means of genetic algorithms, we were able to demonstrate that both optimized NES designs lead to significant passive reduction of the seismic response of the three-story shear-frame structure. An optimized two-NES design (Design II) was capable of (i) reducing the required NES mass at the top floor (compared to Design I); and (ii) improving the overall structural response, as quantified

through a set of objective criteria (these results were discussed in an earlier paper [2] where the study of Designs I and II was performed theoretically).

Both Designs I and II appear to be suitable for structural seismic mitigation against both strong, near-field earthquakes and far-field earthquakes of modest intensity.

Acknowledgment

The support of this work by the National Science Foundation through Grant no. CMS 03-24433 is gratefully acknowledged.

Appendix A. Evaluation criteria for assessing the effectiveness of the proposed seismic mitigation designs

In all criteria [8] defined below, quantities in the denominator refer to the uncontrolled structure, whereas those in the numerator correspond to the controlled one; $u_i(t)$ denotes the absolute displacement of the ith store, η the set of horizontal displacements, $d_i(t)$ the ith interstory drift, and h_i the height of each of the associated story; $\|\cdot\| = \left\{\int_0^{t_f}(\cdot)^2\,\mathrm{d}t\right\}^{1/2}$ denotes the L_2-norm, with t_f being a time interval sufficiently large to allow the response of the structure to attenuate to less than 0.1% of its maximum value.

Evaluation criterion	Related structural response variable	Expression
J_1	Maximum absolute floor displacement (with respect to ground)	$J_1 = \max_{\text{earthquakes}}\left\{\dfrac{\max_{t\ i\in\eta}\lvert u_i(t)\rvert}{u^{\max}}\right\}$
J_2	Maximum interstory drift	$J_2 = \max_{\text{earthquakes}}\left\{\dfrac{\max_{t,i}\lvert d_i(t)\rvert/h_i}{d_n^{\max}}\right\}$
J_3	Maximum absolute floor acceleration (with respect to ground)	$J_3 = \max_{\text{earthquakes}}\left\{\dfrac{\max_{t\ i\in\eta}\lvert \ddot{u}_{ai}(t)\rvert}{\ddot{u}_a^{\max}}\right\}$
J_4	Maximum inertial force at each dof	$J_4 = \max_{\text{earthquakes}}\left\{\dfrac{\max_t\left\lvert\sum_{i\in\eta} m_i\ddot{u}_{a\eta i}(t)\right\rvert}{F_b^{\max}}\right\}$
J_5	Maximum normed floor displacement with respect to the ground	$J_5 = \max_{\text{earthquakes}}\left\{\dfrac{\max_{i\in\eta}\lVert u_i(t)\rVert}{\lVert u^{\max}\rVert}\right\}$
J_6	Maximum normed interstory drift	$J_6 = \max_{\text{earthquakes}}\left\{\dfrac{\max_{t,i}\lVert d_i(t)\rVert/h_i}{\lVert d_n^{\max}\rVert}\right\}$
J_7	Maximum normed absolute floor acceleration (with respect to ground)	$J_7 = \max_{\text{earthquakes}}\left\{\dfrac{\max_{i\in\eta}\lVert \ddot{u}_{ai}(t)\rVert}{\lVert \ddot{u}_a^{\max}\rVert}\right\}$
J_8	Maximum normed inertial force at each dof	$J_8 = \max_{\text{earthquakes}}\left\{\dfrac{\left\lVert\sum_{i\in\eta} m_i\ddot{u}_{a\eta i}(t)\right\rVert}{\lVert F_b^{\max}\rVert}\right\}$

References

[1] F. Nucera, A.F. Vakakis, D.M. McFarland, L.A. Bergman, G. Kerschen, Targeted energy transfer in vibro-impact oscillators for seismic mitigation, *Nonlinear Dynamics (special issue on Discontinuous Dynamical Systems)* (2006), doi:10.1007/s11071-006-9189-7.

[2] F. Nucera, D.M. McFarland, L.A. Bergman, A.F. Vakakis, Application of broadband nonlinear targeted energy transfers for seismic mitigation of a shear frame: computational results, *Journal of Sound and Vibration* (2006) under review.
[3] D. Quinn, R.H. Rand, The dynamics of resonance capture, *Nonlinear Dynamics* 8 (1995) 1–20.
[4] A.I. Neishtadt, Scattering by resonances, *Celestial Mechanics and Dynamical Astronomy* 65 (1997) 1–20.
[5] A.F. Vakakis, O. Gendelman, Energy pumping in nonlinear mechanical oscillators: part II—resonance capture, *Journal of Applied Mechanics* 68 (2001) 42–48.
[6] D.J. Ewins, *Modal Testing: Theory and Practise*, Advanced Studies Press, London, 2000.
[7] P. Fajfar, T. Vidic, M. Fischinger, A measure of earthquake motion capacity to damage medium-period structures, *Soil Dynamics and Earthquake Engineering* 9 (5) (1990).
[8] B.F. Spencer Jr., R.E. Christenson, S.J. Dyke, Next generation benchmark control problem for seismically excited buildings, *Proceedings of the Second World Conference on Structural Control*, Vol. 2, Wiley, New York, 1999, pp. 1135–1360.
[9] T.P. Le, P. Argoul, Continuous wavelet transform for modal identification using free decay response, *Journal of Sound and Vibration* 277 (2004) 73–100.
[10] D.M. McFarland, L.A. Bergman, A.F. Vakakis, Experimental study of nonlinear energy pumping occurring at a single fast frequency, *International Journal of Non-Linear Mechanics* 40 (2005) 891–899.
[11] A.F. Vakakis, Shock isolation through the use of nonlinear energy sinks, *Journal of Vibration and Control* 9 (1–2) (2003) 79–93.
[12] F. Nucera, Nonlinear Energy Pumping as a Strategy for Seismic Protection, PhD Thesis, University of Calabria at Arcavacata, Rende, Italy, 2005.